Saudi Pharmaceutical Journal 25 (2017) 921–926

Contents lists available at ScienceDirect

Saudi Pharmaceutical Journal

journal homepage: www.sciencedirect.com

Original article

Preparation, characterization, and *in vitro* diffusion study of nonwoven electrospun nanofiber of curcumin-loaded cellulose acetate phthalate polymer

Rramaswamy Ravikumar [a,d], Mani Ganesh [a], Udumansha Ubaidulla [b], Eun Young Choi [c], Hyun Tae Jang [a,*]

[a] Department of Chemical Engineering, Hanseo University, 360 Daegok-ri, Seosan-si 356 706, Chungcheongnam-do, South Korea
[b] C.L. Baid Metha College of Pharmacy, Chennai 97, India
[c] Department of Cosmetology, Hanseo University, 360 Daegok-ri, Seosan-si 356 706, Chungcheongnam-do, South Korea
[d] Department of Advanced Materials and Engineering, Hanseo University, 360 Daegok-ri, Seosan-si 356 706, Chungcheongnam-do, South Korea

ARTICLE INFO

Article history:
Received 15 December 2016
Accepted 8 February 2017
Available online 12 February 2017

Keywords:
Curcumin
Cellulose acetate phthalate
Nanofiber
In vitro
Transdermal

ABSTRACT

Novel curcumin (CUR)-loaded cellulose acetate phthalate (CAP) nonwoven electrospun nanofiber (NF) transdermal mat was developed and evaluated for its *in vitro* CUR diffusion properties. Various CAP solutions from 5 to 20 wt% were tested; 17.5 wt% was found to be a suitable concentration for NF fabrication without defects, such as bubble or ribbon structures. The selected wt% CAP solution was loaded with CUR and electrospun into NFs. The prepared CUR-loaded NFs were characterized using scanning electron microscopy, X-ray diffraction, ultraviolet–visible spectroscopy, thermogravimetric analysis (TGA), and *in vitro* diffusion studies. The as-prepared fibers demonstrated controlled *in vitro* transdermal delivery of CUR for up to 24 h.

1. Introduction

Transdermal drug delivery systems are a promising drug delivery route for treating local skin disorders such as acne and various types of wounds; their applicability can be further extended to delivering drugs that are easily degraded when administered orally and undergo first pass metabolism in the liver. The transdermal route can deliver drugs directly to the systemic circulation in a controlled manner, depending on the polymer selected for delivery. The outermost layer of skin, the stratum corneum, plays a key role in limiting drug diffusion to the bloodstream following transdermal delivery, by acting as a controlling barrier; hence, an effective transdermal system must allow drugs to penetrate this skin barrier and reach targeted cells (Hadgraft and Guy, 1989; Guy et al., 1996). Although parenteral drug delivery systems provide rapid delivery and increased plasma levels within a short duration, they are considered more invasive (Flynn, 1996); in general, transdermal delivery is considered to be a non-invasive system, capable of delivering drugs without the difficulties associated with conventional parenteral formulations. During transdermal application, liphophilic molecules enter the body through intracellular lipids present in the stratum corneum, and water-soluble drugs enter through pores close to hair follicles (Surber et al., 1990).

Commonly, transdermal delivery systems are formulated as transdermal gels, patches and films that play an important role in drug delivery formulations (Rehman and Zulfakar, 2014; Pastore et al., 2015). Drugs are loaded into rate-controlling biodegradable polymers; polyacrylates, poly (vinyl alcohol), poly (acrylic acid), polyacrylamide, polylactides (PLA), polyglycolides (PGA), poly(lactide-co-glycolides) (PLGA), polyanhydrides, polyorthoesters, and natural biopolymers such as chitosan, zein, pectin, and cellulose derivatives (e.g., ethyl cellulose, cellulose acetate, and cellulose acetate phthalate (CAP)) have been reported as suitable formulations for transdermal delivery systems (Upadhyay et al., 2014). CAP has proven capability for formulating transdermal patches with promising drug loading and release performance (Patel et al., 2013; Garg et al., 2016).

In the past two decades, ultra-fine structures including microspheres and nanostructures such as nanoparticles and nanospheres, have been of interest in pharmaceutical science for

* Corresponding author.
E-mail address: htjang@hanseo.ac.kr (H. Tae Jang).
Peer review under responsibility of King Saud University.

Production and hosting by Elsevier

http://dx.doi.org/10.1016/j.jsps.2017.02.004
1319-0164/

formulation of new drug delivery systems, due to their controllable high surface area, surface-to-volume ratio, high porosity, and high drug loading and controlled payload delivering capabilities (Bose et al., 2015). Nanofibers (NFs) are a nanostructure that can be produced by various routes, which have been discussed extensively in the review by Huang et al. (2003). Electrospinning is the most promising technique and can produce NFs with ultrafine diameters and well-ordered surface morphologies. In addition to these applications, the high entrapment efficiency, simultaneous delivery of diverse therapeutics, and ease of formulation provided by polymeric electrospun NFs using synthetic and biological polymers has enabled them to be used in drug-loaded wound dressing preparations, drug and protein delivery, and tissue engineering scaffolds (Croisier et al., 2014; Abdelgawada et al., 2014; Hu et al., 2014; Huaimin et al., 2015; Ganesh et al., 2016; Ravikumar et al., 2016; Saravanakumar et al., 2016).

Curcumin a polyphenolic flavonoid from the rhizomes of *Curcuma longa* Linne (turmeric)., is mainly used as a spice in cooking of Indian recepies. Among the available natural anti-inflammatory agents, curcumin (CUR) has been of interest to biological researchers due to its additional anti-bacterial (Mun et al., 2013; Tyagi et al., 2015; Izui et al., 2016; Moghadamtousi et al., 2014; Sharma et al., 2014) and anti-oxidant (Meng et al., 2013; Yao et al., 2015; Chen et al., 2015; Satish and Dilipkumar, 2015; Kant et al., 2014) properties. The anti-inflammatory action of CUR arises from COX-2 inhibition via decreasing neutrophil infiltration at the inflammatory site. Alongside a direct effect on the polarization of neutrophils and chemotaxis, CUR also reduces concentrations of an important cytokine, TNFα, which normally activates signaling cascades involved in inflammation. CUR can decrease oxidative stress via scavenging reactive oxygen species (ROS) by alleviating the accumulation of melanodialdehyde, superoxide anions, and nitrous oxide (Remya et al., 2016). CUR can also enhance wound healing by promoting the amalgamation of collagen, hexosamin, DNA, and nitrates. In addition to these amalgamations, CUR also has the ability to hasten wound closure by rapid re-epithelialization of the epidermis and exodus of cells such as macrophages, fibroblasts, and myofibroblasts from wound surfaces (Rajesh et al., 2013). Various CUR-loaded transdermal systems have been reported (Patel et al., 2009a,b; Olaru and Olaru, 2010); however, to our knowledge, there have been no studies on NF-based transdermal delivery systems for CUR-loaded formulations.

Considering the advantages of CAP in the development of transdermal delivery systems, and the possibility of delivering CUR through the transdermal route, here we report the development of a novel CAP-based NF preparation loaded with CUR for transdermal application. The effects of CAP weight, the solvent used, and other processing parameters on NF morphology were investigated using scanning electron microscopy (SEM) and other physiochemical characterization procedures. Formulated NFs were characterized using Fourier-transform infrared spectroscopy (FTIR), differential scanning calorimetry (DSC), and thermogravimetric analysis (TGA). *In vitro* diffusion of CUR from the NFs was examined using pig skin as a transdermal barrier.

2. Methods

2.1. Materials

CAP with molecular weight 2534.12 g/mol and CUR were obtained from Sigma-Aldrich (Korea); ethyl acetate (EA) and isopropyl alcohol (IPA) were obtained from Daejung Chemical and Metals (Korea). All other chemicals used were of analytical grade, unless otherwise noted.

2.2. Preparation of nanofibers (NFs)

During the pre-formulation procedure, a range of CAP concentrations (5, 10, 15, 17.5, and 20 wt%) in a 25:75 mixture of IPA and EA, respectively, were prepared and loaded into the sample feeder used for nanofabrication. Electrospinning was conducted using the procedure described below. Similarly, CUR-loaded fiber was prepared by adding 10% CUR with respect to the total amount of CAP, made into a solution using the same solvent system, and fabricated into NFs using the same procedure.

2.3. Preparation of NFs by electrospinning

The plain CAP and CUR-loaded CAP NFs were prepared in similar manner. The prepared CAP and CUR/CAP solutions were placed into a 10-mL syringe, fitted with a blunt metal needle (21 gauge). The distance between the needle and an aluminum foil-wrapped drum collector was maintained at 15 cm. An approximately 12-kV high-voltage direct current was supplied between the drum and the needle; after a series of trials, the solution feedrate from the needle was fixed at 1.5 mL h^{-1}. The collector was rotated at a speed of 30 rpm. The fabricated NFs were collected carefully from the collector, dried at room temperature for 48 h to ensure complete evaporation of the solvent, and then weighed and stored in a light-protected container at room temperature until further investigation. Images of the optimized NF mats on adhesive patches are provided in Supplementary Material Fig. S1.

2.4. Characterization

The surface morphology of the prepared NFs was evaluated using SEM (JEOL JSM 5600, Japan). A square-shaped NF sample of suitable size was placed on double-sided adhesive tape on the aluminum stub of the SEM; samples were then coated with gold plasma sputter (Sputter Coater-108 Auto, Cressington).FTIR spectra were obtained for the pure polymer, CUR physical mixture, and NF samples using a Nicolet 6700 FT-IR spectrometer at room temperature via the KBr pellet technique. In total, 20 scan cycles were obtained at 4-cm^{-1} resolution over the range of 4000–400 cm^{-1}. To determine the crystalline nature of the polymer, CUR, and CUR-loaded polymer, X-ray diffraction (XRD) images were recorded using a Rigaku Miniflex diffractometer with Cu Kα radiation (λ = 1.54 Å), a 2θ range of 10–80 with a 0.1° step size, and a 1-s step time. A Scinco DSC N 650 system was used to record DSC traces of pure CAP, CUR, CAP NF, and CAP-CUR NF with a heating rate of 10 °C/min under a helium atmosphere (40 mL/min) to evaluate crystalline changes in CUR after fabrication. To determine the mechanical stability of the formulated NFs, TGA was conducted using Scinco N-1000 analyzer under N_2 atmosphere; here 10-mg fiber samples were heated in platinum pan from 25 to 800 °C at a rate of 10 °C/min.

2.5. Drug entrapment efficiency

The amount of the drug entrapped in the formulated NF mat was evaluated by drying the CUR-loaded CAP NF in a hot air oven at 40 °C. After drying, the weight of the NF mat was measured, then the sample was dissolved in the respective solvent (IPA:EA; 25:75 for the CAP NF). The amount of CUR present in the solvent was measured using ultraviolet–visible (UV–Vis) spectrometry at 420 nm; the theoretical value of CUR added to the CAP NF solution before electrospinning is given below in terms of the entrapment efficiency (Saravanakumar et al., 2016):

$$\text{Entrapment efficiency } (\%) = \frac{\text{Wt of max. drug release}}{\text{Wt of drug added}} \times 100 \quad (1)$$

2.6. Degree of swelling

The swelling behavior of the CUR-loaded CAP NF was analyzed by placing a known weight of the NF mat in a phosphate buffer (pH: 7.4) at 37 °C. The immersed mat was then removed from the medium at a defined time. The % degree of swelling was calculated using the following Eq. (2) (Saravanakumar et al., 2016):

$$\text{Degree of swelling} = \frac{W_s - W_d}{W_d} \times 100 \quad (2)$$

where w_s is the weight of the swollen NF sample (wiped with tissue paper for drying) and w_d is the dried weight of the sample immersed in the medium. The weight of the swollen NF was calculated after drying in a hot air oven at 40 °C for 10 min to obtain the constant weight of the sample.

2.7. In vitro diffusion study

In vitro skin permeation studies were carried out using Franz diffusion cell with a receptor compartment capacity of 20 mL. Excised pig abdominal skin collected from an abattoir was cleaned and mounted between the donor and receptor compartment of the diffusion cell. The formulated patches were placed over the skin and covered with paraffin film. The receptor compartment of the diffusion cell was filled with a phosphate buffer of pH 7.4 contained 20% alcohol. The whole assembly was fixed on a magnetic stirrer. The solution in the receptor compartment was stirred continuously using a magnetic bead at 50 rpm, with the temperature maintained at 32 ± 0.5 °C. The samples were withdrawn at different time intervals and analyzed for drug content using a UV–Vis spectrophotometer at 420 nm. The receptor phase was replenished with an equal volume of the same medium. The cumulative permeating drug amount per square centimeter of patch was plotted as a function of time.

2.8. Statistical evaluation

The drug diffusion and swelling behaviors were statistically evaluated in terms of the mean and its standard deviation (mean ± SD). The fitting values were obtained using commercially available software Origin 8.5 (Origin Lab Inc., Northampton, MA, USA).

3. Results and discussion

3.1. Characterization

Earlier reports on CAP nanofiber fabrication have discussed the usage of various solvent systems such as mixtures of acetone/water (85:15 at 15 wt% CAP), 2-methoxyethanol, 2-methoxyethanol/acetone/water (50:42.5:7.5 at 25% CAP), acetone/ethanol (9:1), DMF/THF/acetone (3:3:4), THF/acetone (1:1), THF/ethanol (1:1), and chloroform/methanol (1:1) (Olaru and Olaru, 2010; Shrestha et al., 2016). With a simple acetone/water mixture, the fabricated fiber had a twisted, rough morphology, while the 2-methoxy ethanol combination resulted in smooth fiber morphology but required higher CAP concentrations to attain the viscosity required for spinning (Olaru and Olaru, 2010). Shrestha et al. (2016) also suggested the use of an acetone/ethanol (9:1) system with 15% polymer produced fiber for good morphology; however, the structure they observed showed beads and rough surfaces over the nanofiber. Hence, in our study, we extended the search for new solvent combinations to obtain smooth, uniformly sized NFs. We found that 75:25 EA: IPA combination was ideal for spinning CAP. Further, the slow and constant volatility of IPA resulted in slow polymer relaxation during drying, which assists in obtaining a smooth morphology, in contrast to shock-induced fast drying with a highly volatile solvent such as acetone and 2-methoxyethanol and twisting, branching, ribbon-like structures that may be created by low volatility solvents such as dimethyl formamide (Olaru and Olaru, 2010).

Fig. 1 shows the SEM morphological characteristics of NFs formulated using different concentrations of CAP; fibers formed using low polymer concentrations (5, 10, and 15 wt%) resulted in beads and branching structure, implying that these concentrations have insufficient viscosity to form continuous NFs. In addition, the Taylor cones at these concentrations were not properly formed, and significant dropping of the polymer solution was observed during electrospinning. The fiber formed with 17.5 wt% CAP concentration resulted in a smooth, rounded morphology, without any beads or

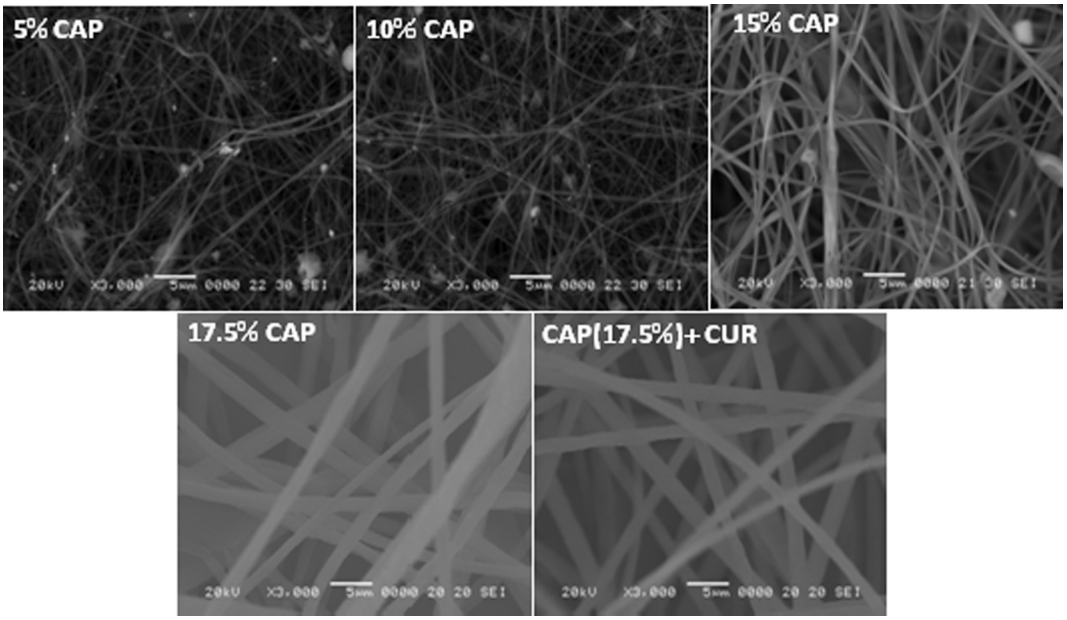

Fig. 1. SEM images of nanofibers obtained with various polymer concentration and CUR loaded nanofiber.

branching and with a size of 300 ± 20 nm. Hence, this concentration was used for further CUR-loading into the CAP NF.

Fig. 2(a) shows the FTIR spectrum of pure CAP, with characteristic bands at 1056, 1252, 1600, 1732, and 2938 cm^{-1}, respectively, associated with —C—O— and —C—O—C— stretching, the —C=C— conjugated vinyl aromatic ring, the —C=O— carboxyl group, and asymmetric and symmetric stretching of methyl —C—H groups (Manjunath and Sailaja, 2014). However, for CUR, as shown in Fig. 2(b), characteristic transmittance bands were observed at 1581, 1511, 1279, and 1152 cm^{-1} corresponding to stretching C=C vibrations of benzene, aromatic C—O stretching of (—OMe and —OH), and C—O—C stretching (—OMe), respectively (Zhao et al., 2015). Further, characteristic bands for phenolic —OH and conjugated ketonic —C=O vibrations were observed at 3451 cm^{-1} (1620 cm^{-1}) and 1562 cm^{-1} (1420 cm^{-1}) respectively (Parize et al., 2012). In the case of the CAP and CUR physical mixture (Fig. 2(c)), individual characteristic peaks were observed, but with low intensity due to improper mixing caused by the ridged plastic structure of CAP. Hence, no polymer drug interaction on the physical mixture was observed.

Fig. 2(d) shows the FTIR spectrum for CAP NF; all of the major bands were matched exactly those of pure CAP. The peak at 3500 cm^{-1} was attributed to -OH stretching of water or —OH of IPA; this band was not observed with pure CAP, and so may have arisen from the moisture content of IPA or its alcoholic —OH group.

For CAP-CUR NF [Fig. 2(e)], the FTIR peaks for CAP dominated over CUR bands; only a few CUR peaks, such as those at 1279 and 1152 cm^{-1} for aromatic C—O stretching of (—OMe and —OH) and C—O—C stretching (—OMe), respectively, were observed. The aromatic stretching C=C vibration peak for benzene (1581 cm^{-1}) is common in both CAP and CUR and, hence, these overlapped. The polymer has no functional group that can interact with CUR; as such, no reactive interaction bands were observed.

Fig. 3(a) shows the XRD pattern for CUR (pristine), in which characteristic peaks for crystalline CUR were observed at 2θ = 14.37,18.78, 20.78, 23.08, and 29.26. In the case of CAP fiber showed the typical amorphous pattern in XRD (Fig. 3(b)). Upon encapsulation of CUR with the polymer during NF fabrication, it loses its crystallinity (Fig. 3(c)), as evidenced by the absence of characteristic peaks of pristine CUR (Fig. 3(a)). The loss of the crystalline structure of CUR in NFs indicates fine dispersion and successful encapsulation. Similar results have also been reported in earlier studies of CUR encapsulation in other polymers (Pan et al., 2013; Patel et al., 2010).

Fig. 4 shows DSC results for the pure polymer, CUR, and the NFs. The smooth curve of CAP indicates its existence in an amorphous form, with thermal stability up to 300 °C. A sharp melting endotherm peak was observed at 177.3 °C for pristine CUR similar

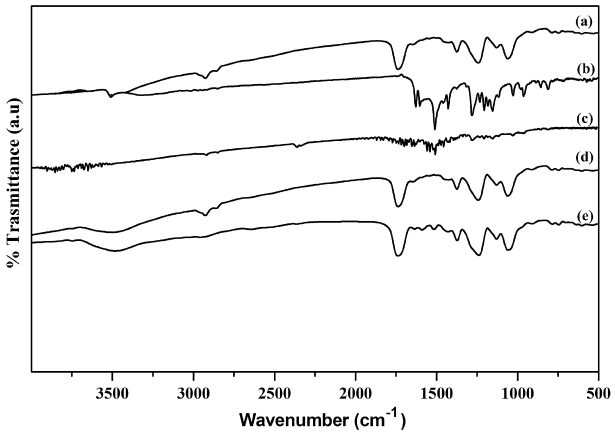

Fig. 2. FTIR spectrum of (a) CAP, (b) CUR, (c) CAP and CUR physical mixture, (d) CAP-NF (e) CUR - CAP-NF.

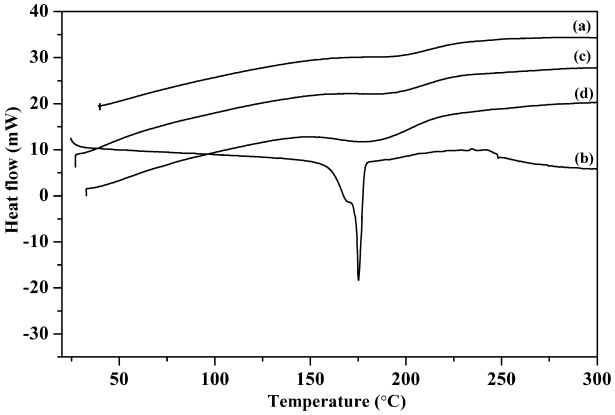

Fig. 4. DSC traces of (a) CAP, (b) CUR, (c) CAP-NF and (d) CUR - CAP-NF.

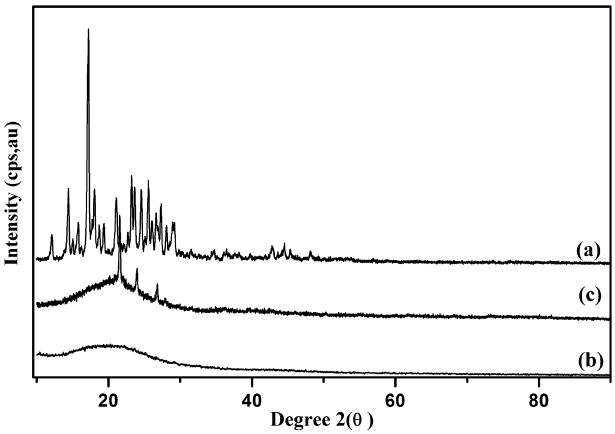

Fig. 3. XRD traces of (a) CUR, (b) CAP and (c) CUR - CAP-NF.

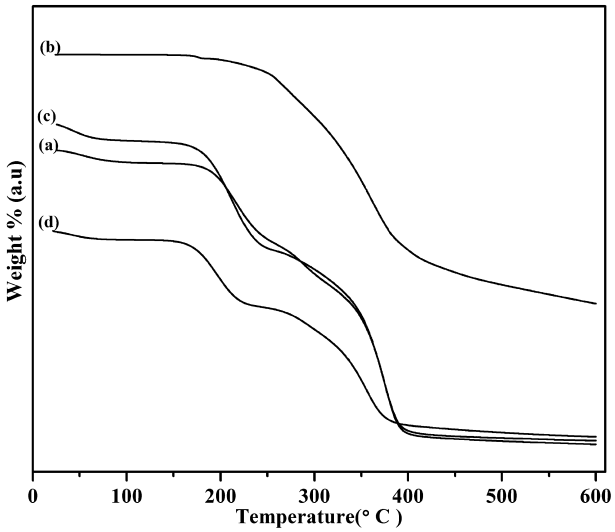

Fig. 5. TGA traces of (a) CAP, (b) CUR, (c) CAP-NF and (d) CUR - CAP-NF.

to that observed in previous reports (Zhao et al., 2015; Jasim and Talib, 1992); the absence of an endothermic peak for CUR in NF confirms the loss of crystallinity, as shown in the XRD results. Further, this confirms the fine dispersion of CUR over the fibers.

Fig. 5 shows the thermal behavior of CAP, CUR, CAP NF, and CAP-CUR NF. Among these thermograms Fig. 5(a), (c), and (d) show the stability and degradation patterns of CAP, CAP-NF, and CAP-CUR NF, respectively, with similar weight loss patterns. All of the patterns indicated a ~3% weight loss below 100 °C, which represents the water loss from the polymer and polymer composite. A loss of ~25% was observed from 180 to 200 °C; this may be due to the loss of acetyl and phthaloyl moieties from the polymer. A significant weight loss of ~50% was observed at nearly 300 °C, which implies degradation of the cellulose backbone of the polymer. A similar weight loss pattern has been reported in previous studies on CAP (Roxin et al., 1998). As the polymer concentration is high in CUR-loaded NF, it did not exhibit the same specific weight loss patterns as CUR alone. The TGA of CUR alone showed degradation starting at ~300 °C(Fig. 5(b), extending up to 550 °C; a similar weight loss pattern has been reported for CUR in previous studies (Chena et al., 2014).

3.2. Drug entrapment and degree of swelling

From the UV–Vis spectrophotometric estimation, the amount of CUR loaded into the NF formulated with 17.5% CAP concentration was 96.7%. Fig. 6 shows the swelling behavior of the formulated NF(a) before and after loading with CUR(b). In both cases, a similar type of swelling behavior was noted, with about 400% weight gain from 1 to 12 h, due to water engulfed in the pores; then after, the weight of the fiber began to decrease. The observed weight loss may be due to slow hydrolysis of phthalate and acetate moieties from the cellulosic backbone.

3.3. In vitro diffusion studies

In vitro diffusion profiling is an important tool that predicts in advance how the drug will behave *in vivo*. The results of the *in vitro* skin permeation studies of CUR from NF transdermal patches are shown in Fig. 7. The cumulative amount of drug diffusion from the 17.5 wt% CAP formulation was 309.02 μg/cm^2 at 24 h. The cumulative amount of drug permeating per square centimeter of patch through the pig skin over time followed mixed zero-order/first-order kinetics. The *in vitro* diffusion profiles for the formulations did not fit closely with either zero-order (r^2 = 0.8962) or

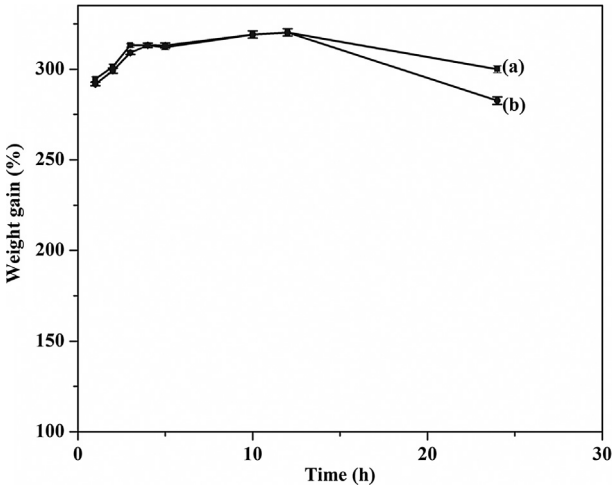

Fig. 6. Swelling behavior of (a) CAP-NF and (b) CAP -CUR-NF.

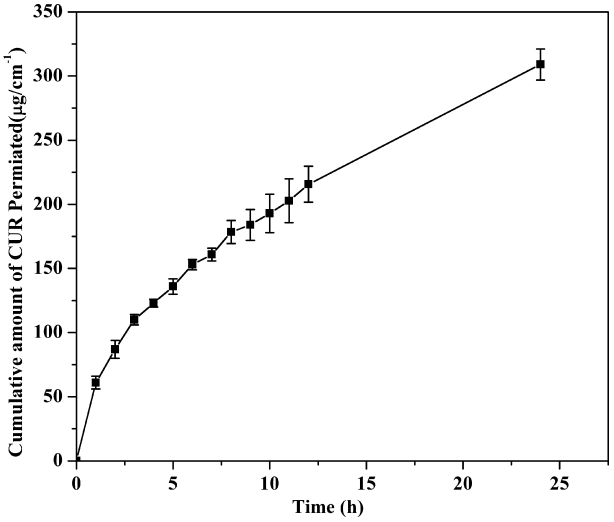

Fig. 7. In-vitro diffusion of curcumin from CAP nanofibers.

first-order kinetics (r^2 = 0.973) (See Supplementary Fig. S2); however, the diffusion profile of the formulated patch followed Higuchi's equation (r^2 = 0.9989), which indicates that drug permeation from the patch is governed by a diffusion mechanism (Higuchi, 1961). As many diffusion processes can be represented by coupling of a Fickian and non-Fickian mechanism, to describe the controlled diffusion of drugs from polymer matrices, Ritger and Peppa introduced the power law equation $M_t/M_\infty = Kt^n$, where M_t is the amount of drug released at time t, M_∞ is the nominal total amount of drug released at K the kinetic constant, and *n* is the diffusion exponent that is used to characterize the release mechanism (Ritger and Peppas, 1987). The value of *n* can be calculated from the slope of ln ($M_t/M\infty$) versus ln *t* and can indicate the operating diffusion mechanism. The *n* value (0.504) obtained using this equation indicated that the Fickian mechanism dominated in all formulated NFs. In this context, the results obtained from the Fickian mechanism support the results of Higuchi's equation. Thus, we can conclude that the patches demonstrate a diffusion-dominated mechanism for drug delivery.

4. Conclusions

A novel CAP nonwoven NF mat was fabricated using EA: IPA as the solvent system, and the mat was evaluated for its *in vitro* CUR transdermal permeation capability. The NFs had an average diameter of 300 nm, with a narrow size distribution. FTIR and XRD results confirmed CUR loading of the NF material. A concentration of 17.5 wt% CAP was found to be ideal for successful NF formation with smooth structural features and slow sustained diffusion of the loaded CUR. Further, this study provides insight into the development and utilization of CAP NFs as a controlled transdermal delivery system for drugs that may be degraded when administered orally and require sustained systemic delivery through the skin.

Acknowledgement

The authors gratefully acknowledge the financial support received from Hanseo University Intramural Research Grant 2016 and extend their thanks to the National Research Foundation of Korea (NRF), funded by the Ministry of Science, ICT and Future Planning (Grant No. 2014-004694), South Korea for their partial financial support.

Appendix A. Supplementary material

Supplementary data associated with this article can be found, in the online version, at http://dx.doi.org/10.1016/j.jsps.2017.02.004.

References

Abdelgawada, A.M., Hudsona, S.M., Rojasb, O.J., 2014. Antimicrobial wound dressing nanofiber mats from multicomponent (chitosan/silver-NPs/polyvinyl alcohol) systems. Carbohydr. Polym. 100 (2014), 166–178.

Chen, X., Zou, L.Q., Niu, J., Liu, W., Peng, S.F., Liu, C.M., 2015. The stability, sustained release and cellular antioxidant activity of curcumin nanoliposomes. Molecules 20 (8), 14293–14311.

Chena, Z., Xia, Y., Liao, S., Huang, Y., Li, Y., He, Y., Tong, Z., Li, B., 2014. Thermal degradation kinetics study of curcumin with nonlinear methods. Food Chem. 15, 81–86.

Croisier, F., Atanasova, G., Poumay, Y., Jérôme, C., 2014. Polysaccharide-coated PCL nanofibers for wound dressing applications. Adv. Healthcare Mater. 3 (12), 2032–2039.

Flynn, G.L., 1996. Cutaneous and transdermal delivery: processes and systems of delivery. In: Banker, G.S., Rhodes, C.T. (Eds.), Modern Pharmaceutics. Marcel Dekker, New York, p. 187.

Ganesh, M., Aziz, A. Sch, Ubaidulla, U., Hemalatha, P., Saravanakumar, A., Ravikumar, R., Peng, M.M., Choi, E.Y., Jang, H.T., 2016. Sulfanilamide and silver nanoparticles-loaded polyvinyl alcohol-chitosan composite electrospun nanofibers: synthesis and evaluation on synergism in wound healing. J. Ind. Eng. Chem. 39, 127–135.

Garg, A., Rai, G., Lodhi, S., Jain, A.P., Yadav, A.K., 2016. In-vitro and in-vivo assessment of dextran-appended cellulose acetate phthalate nanoparticles for transdermal delivery of 5-fluorouracil. Drug Deliv. 23 (5), 1525–1535.

Guy, R., Powell, M., Fix, J., 1996. Current status and future prospects of transdermal drug delivery. Pharm. Res. 13 (12), 1759–1768.

Hadgraft, J., Guy, R.H., 1989. Transdermal Drug Delivery: Developmental Issues and Research Initiatives. Marcel Dekker Eds, New York, p. 324.

Higuchi, T., 1961. Rate of release of medicaments from ointment bases containing drugs in suspension. J. Pharm. Sci. 50 (10), 874–875.

Hu, X., Liu, S., Zhou, G., Huang, Y., Xie, Z., Jing, X., 2014. Electrospinning of polymeric nanofibers for drug delivery applications. J. Control. Release 185, 12–21.

Huaimin, W., Youzhi, W., Xiaoli, Z., Yawen, H., Xiaoyong, Y., Linsha, M., Hao, Z., Jiafu, L., Qian, L., Zhimou, Y., 2015. Supramolecular nanofibers of self-assembling peptides and proteins for protein delivery. Chem. Commun. 51, 14239–14244.

Huang, Z.-M., Zhang, Y.-Z., Kotaki, M., Ramakrishna, S., 2003. A review on polymer nanofibers by electrospinning and their applications in nanocomposites. Compos. Sci. Technol. 63 (15), 2223–2253.

Izui, S., Sekine, S., Maeda, K., Kuboniwa, M., Takada, A., Amano, A., Nagata, H., 2016. Antibacterial activity of curcumin against periodontopathic bacteria. J. Periodontol. 87 (1), 83–90.

Jasim, F., Talib, T., 1992. Some observations on the thermal behaviour of curcumin under air and argon atmospheres. J. Therm. Anal. Calorim. 38 (11), 2549–2552.

Kant, V., Gopal, A., Pathak, N.N., Kumar, P., Tanda, S.K., Kumar, D., 2014. Antioxidant and anti-inflammatory potential of curcumin accelerated the cutaneous wound healing in streptozotocin-induced diabetic rats. Int. Immunopharmacol. 20 (2), 322–330.

Manjunath, L., Sailaja, R.R.N., 2014. PMMA–cellulose acetate phthalate nanocomposites reinforced with silane-treated nanoclay. Cellulose 21 (3), 1793–1802.

Meng, B., Li, J., Cao, H., 2013. Antioxidant and antiinflammatory activities of curcumin on diabetes mellitus and its complications. Curr. Pharm. Des. 19 (11), 2101–2113.

Moghadamtousi, S.Z., Kadir, H.A., Hassandarvish, P., Tajik, H., Abubakar, S., Zandi, K., 2014. A review on antibacterial, antiviral, and antifungal activity of curcumin. BioMed Res. Int., 1–12

Mun, S.H., Joung, D.K., Kim, Y.S., Kang, O.H., Kim, S.B., Seo, Y.S., Lee, D.S., Shin, D.W., Kweon, K.T., Kwon, D.Y., 2013. Synergistic antibacterial effect of curcumin against methicillin-resistant *Staphylococcus aureus*. Phytomedicine 20 (8–9), 714–718.

Olaru, N., Olaru, L., 2010. Electrospinning of cellulose acetate phthalate from different solvent systems. Ind. Eng. Chem. Res. 49 (4), 1953–1957.

Pan, K., Zhong, Q., Baek, S.J., 2013. Enhanced dispersibility and bioactivity of curcumin by encapsulation in casein nanocapsules. Agric. Food Chem. 61 (25), 6036–6043.

Parize, A.L., Stulzer, H.K., Laranjeira, M.C.M., Brighente, I.M. da C., Tereza, C.R.de., 2012. Evaluation of chitosan microparticles containing curcumin and crosslinked with sodium tripolyphosphate produced by spray drying. Quim. Nova 35 (6), 1127–1132.

Pastore, M.N., Kalia, Y.N., Horstmann, M., Roberts, M.S., 2015. Transdermal patches: history, development and pharmacology. Br. J. Pharmacol. 172 (9), 2179–2209.

Patel, A., Hu, Y., Tiwari, J.K., Velikov, K.P., 2010. Synthesis and characterisation of zein–curcumin colloidal particles. Soft Matter 6 (24), 6192–6199.

Patel, H.V., Bhatt, J.D., Patel, N.K., 2013. Design and development of transdermal drug delivery for anti-hypertensive drug using different polymeric system. Int. J. Pharm. Chem. Sci. 2 (2), 942–949.

Patel, N.A., Patel, N.J., Patel, R.P., 2009a. Design and evaluation of transdermal drug delivery system for curcumin as an anti-inflammatory drug. Drug Dev. Ind. Pharm. 35 (2), 234–242.

Patel, N.A., Patel, N.J., Patel, R.P., 2009b. Formulation and evaluation of curcumin gel for topical application. Pharm. Dev. Technol. 14 (1), 83–92.

Bose, R.J.C., Arai, Y., Ahn, J.C., Park, H., Lee, S.-H., 2015. Influence of cationic lipid concentration on properties of lipid–polymer hybrid nanospheres for gene delivery. Int. J. Nanomed. 10, 5367–5382.

Rajesh, L.T., Shashwat, S., Radha, K.M., 2013. Skin regenerative potentials of curcumin. Biofactors 39 (1), 141–149.

Ravikumar, R., Peng, M.M., Abidov, A., Babu, C.M., Vinodh, R., Palanichamy, M., Choi, E.Y., Jang, H.T., 2016. Nanofibrous polymers blend of fluorouracil loaded chitosan-hydroxy ethyl cellulose/poly vinyl alcohol: synthesis and characterization. Int. J. Bio-Sci. Bio-Technol. 8 (2), 295–306.

Rehman, K., Zulfakar, M.H., 2014. Recent advances in gel technologies for topical and transdermal drug delivery. Drug Dev. Ind. Pharm. 40 (4), 433–440.

Remya, S., Somasundaram, A., Rajarajan, A.T., Vengadeshprabhu, K., Kenichi, W., 2016. Curcumin as a therapeutic agent in the chemoprevention of inflammatory bowel disease. Drug Discov. Today 21 (5), 843–849.

Ritger, P.L., Peppas, N.A., 1987. A simple equation for description of solute release. II. Fickian and anomalous release from swellable devices. J. Control. Release 5 (1), 37–42.

Roxin, P., Karlsson, A., Singh, S.K., 1998. Characterization of cellulose acetate phthalate (CAP). Drug Dev. Ind. Pharm. 24 (11), 1025–1041.

Saravanakumar, A., Ganesh, M., Jang, J.H., Yun, H.C., Jung, H.L., Seung, S.O., Han, E.C., Han, D.K., Jang, H.T., 2016. Preparation and characterization of gatifloxacin-loaded alginate/poly (vinyl alcohol) electrospun nanofibers. Artif. Cells, Nanomed. Biotechnol. 44 (3), 847–852.

Satish, B.N., Dilipkumar, P., 2015. Free radicals, natural antioxidants, and their reaction mechanisms. RSC Adv. 5, 27986–28006.

Sharma, G., Raturi, K., Dang, S., Gupta, S., Gabrani, R., 2014. Combinatorial antimicrobial effect of curcumin with selected phytochemicals on *Staphylococcus epidermidis*. J. Asian Nat. Prod. Res. 16 (5), 535–541.

Shrestha, R., Palat, A., Punnoose, A.M., Joshi, S., Ponraju, D., Paul, S.F.D., 2016. Electrospun cellulose acetate phthalate nanofibrous scaffolds fabricated using novel solvent combinations biocompatible for primary chondrocytes and neurons. Tissue Cell 18 (6), 634–643.

Surber, C., Wilhelm, K.P., Hori, M., 1990. Optimization of topical therapy: partitioning of drugs into stratum corneum. Pharm. Res. 7 (12), 1320–1324.

Tyagi, P., Singh, M., Kumari, H., Kumari, A., Mukhopadhyay, K., 2015. Bactericidal activity of curcumin I is associated with damaging of bacterial membrane. PLoS One 10 (3), 1–15.

Upadhyay, G., Verma, S., Parvez, N., Sharma, P.K., 2014. Recent trends in transdermal drug delivery system – a review. Adv. Biol. Res. 8 (3), 131–138.

Yao, M., Yang, L., Wang, J., Sun, Y.L., Dun, R.L., Wang, Y.J., Cui, X.J., 2015. Neurological recovery and antioxidant effects of curcumin for spinal cord injury in the rat: a network meta-analysis and systematic review. J. Neurotrauma 32 (6), 381–391.

Zhao, Z., Xie, M., Li, Y., Chen, A., Li, G., Zhang, J., Hu, H., Wang, X., Li, S., 2015. Formation of curcumin nanoparticles via solution enhanced dispersion by supercritical CO_2. Int. J. Nanomed. 10 (1), 3171–3181.